Electronic Supplementary Information

Interfacial aspect of Bi_2O_3/CeO_x heterostructure catalysts for HCOOH production from CO_2 electroreduction

*Chaochen Wang,[a] Ruichao Pang,[a] Zhenping Pan,[a] Yihua Zhu,[*a] Chunzhong Li,[b] Bin Liu,[*c] and Jianhua Shen[*a]*

[a] Shanghai Engineering Research Center of Hierarchical Nanomaterials, Key Laboratory for Ultrafine Materials of Ministry of Education, Frontiers Science Center for Materiobiology and Dynamic Chemistry, School of Materials Science and Engineering, East China University of Science and Technology Shanghai 200237, China

[b] School of Chemical Engineering, East China University of Science and Technology, Shanghai 200237, China

[c] State Key Laboratory of Chemical Resource Engineering, College of Chemistry, Beijing University of Chemical Technology, Beijing 100029, China.

E-mails: yhzhu@ecust.edu.cn (Yihua Zhu); binliu@buct.edu.cn (Bin Liu); jianhuashen@ecust.edu.cn (Jianhua Shen)

Supplementary methods

Chemicals

Bismuth trichloride ($BiCl_3$) and Cerium (Ⅲ) chloride heptahydrate ($CeCl_3 \cdot 7H_2O$) were purchased from Shanghai Macklin Biochemical Co., Ltd. 1,2-Epoxypropane (PO) was purchased from Shanghai Titan Technology Co., Ltd. Nafion solution (5 wt%) and Nafion 117 membrane were obtained from Sigma-Aldrich. Carbon fiber paper was purchased from Toray. Deuterium oxide (D_2O) was purchased from Shanghai Aladdin Biochemical Technology Co., Ltd. Potassium bicarbonate ($KHCO_3$) was purchased from Tianjin Damao Chemical Reagent Co., Ltd. All the chemicals were of analytical grade.

Preparation of working electrodes

The synthesized catalyst (1 mg) was dispersed in a mixed solution of ethanol (75 μL), deionized water (19 μL), and Nafion solution (6 μL, 5 wt%), and then sonicated for 30 min to form a homogeneous ink. The above ink was uniformly spread on carbon fiber paper (1×1 cm^2) to prepare the working electrode.

Electrochemical measurements and products analysis

Electrochemical measurements were performed by assembling three-electrode system in a H-type cell separated by Nafion 117 membrane in an electrochemical workstation (CHI 660E). The prepared catalyst electrode , carbon rod and Ag/AgCl electrode (3.0 M KCl) were used as working electrode, counter electrode and reference electrode, respectively. 0.5 M $KHCO_3$ (pH $\approx$ 7.36) was used as the electrolyte. All potentials were calibrated to the reversible hydrogen electrode (RHE) reference scale using $E_{RHE} = E_{Ag/AgCl} + 0.059 \times pH + 0.196$. Linear sweep voltammetry (LSV) tests were carried out with a scanning rate at 10 mV s^{-1} from -0.1 to -1.2 V (versus RHE) in CO_2 or Ar saturated electrolyte. A pure CO_2 gas (99.99%) was bubbled into the aqueous electrolyte (40 mL) for 30 min before each experiment. The current was normalized by the geometric surface area of working electrode. The electrolyte in the cathodic compartment was stirred at a rate of 200 rpm. During the experiments, CO_2 gas was delivered at an average rate of 5 mL/min and routed directly into the gas sampling loop of a gas chromatograph (shiweipx GC-2060) equipped with a molecular sieve TDX-01 and Al_2O_3 capillary column with Ar (Ultra high purity) flowing as a carrier gas. The

separated gas products were analyzed by a thermal conductivity detector (TCD) and a flame ionization detector (FID). The electrochemical surface area, ECSA = $R_f S$, where S stands for the real surface area of the smooth metal electrode, which was generally equal to the geometric area of carbon fiber paper (in this work, S=1 cm^2). The roughness factor R_f was estimated from the ratio of double-layer capacitance Cdl for the working electrode and the corresponding smooth metal electrode (Specific capacitance for carbon was reported as 40 μF cm^{-2}[26]). Therefore, $R_f = C_{dl}/40$ μF cm^{-2}. The C_{dl} was determined by measuring the capacitive current associated with double-layer charging from the scan-rate dependence of cyclic voltammetric stripping. The potential window of cyclic voltammetric stripping was 0.1 V to 0 V versus RHE. The scan rates included 5 mV/s, 10 mV/s, 20 mV/s, 40mV/s, and 60 mV/s. The C_{dl} was estimated by plotting the $\Delta j = (j_a - j_c)$ at 0.50 V (where j_c and j_a are the cathodic and anodic current densities, respectively) versus RHE against the scan rates, in which the slope was twice that of C_{dl}.

For gaseous products, the Faradaic efficiency (FE_{gas}) was calculated as follows:

$$FE_{gas} = \frac{q_g}{q_{tot}} \times 100\% = \frac{v \times V \times N \times F}{60 \times 24000 \times j} \times 100\% \quad \textbf{(1)}$$

Where v was the CO_2 flow rate, V was the measured product concentration in the GC sample loop, N = 2 was the number of electron transfers to form a molecule of CO or H_2, F was the Faraday constant (96485 C mol^{-1}), and j was the total current.

For liquid products, the following method was used for the calculation of Faradaic efficiency (FE_{liquid}):

$$FE_{liquid} = \frac{q_l}{q_{tot}} \times 100\% = \frac{F \times c_l \times V_{cell} \times n_l}{q_{tot}} \times 100\% \quad \textbf{(2)}$$

Where c_l (mol L^{-1}) was the concentration of formate that was calculated from ^{1}H NMR spectroscopy, F was Faraday constant, Vcell (L) was the electrolyte volume in the cell, and to (C) was the passed total charge.

Characterizations

Transmission electron microscopy (TEM) was carried out on a Jeol JEM-2100 microscope operating at 200 kV. X-ray powder diffractometer equipped with a Philips X`Pert Pro Super diffractometer equipped with Cu Kα radiation (λ=1.54**06** Å) was used for collecting X-ray diffraction pattern (XRD) of samples. The X-ray photoelectron spectra (XPS) were acquired by photoelectron spectrometer (VG ESCA 2000) with an Mg anode. All data were corrected using the C 1s peak at 284.6 eV as an internal standard. The high-angle annular dark-field scanning transmission electron microscopy (HAADF-STEM) was performed on a JEOL JEM-ARF300F TEM/STEM **.**

Density functional theory (DFT) calculations

All the DFT calculations were conducted using the Dmol3 module of Materials Studios 2017.[1] The electronic exchange and related energy were treated using the Perdew, Burke and Ernzerhof (PBE) functional within the generalized gradient approximation (GGA).[2] The conductor like screening model (COSMO) method was adopted to consider the electrostatic interaction of adsorbate and water solvent.[3] The DFT semi-core pseudo potentials (DSPPs) core treatment with the relativistic effects were implemented to consider the core-electron (e^-) interaction, which superseded core e^- by a single valid electricpotential to simplify the calculations.[4] The numerical basis set of double numerical plus polarization (DNP) was utilized. Thermal smearing of orbital occupation is set to 0.005 Ha (1 Ha = 27.21 eV). A 3×3×1 Monkhorst-Pack grid of special k-points was used for Brillouin zone integration. The SCF density convergence tolerance was 1×10^{-5} Ha. The maximum force, displacement, and energy of geometry optimal convergence tolerance are 0.004 Ha/Å, 0.005 Å, and 2×10^{-5} Ha. The standard hydrogen electrode (SHE) model was calculated the Gibbs free energy change (ΔG) for each basic step. Based on this method, the ΔG value can be determined as follows: $\Delta G = \Delta E + \Delta ZPE - T\Delta S + \int CpdT$, where ΔE is the electronic energy difference calculated from DFT, ΔZPE is the change in zero-point energies, T is the ambient temperature, Cp is the heat capacity and ΔS is the entropy change. The thermodynamic properties of gas-phase molecules and ZPE contribution of adsorbed species are obtained through vibrational frequencies. The computational hydrogen electrode (CHE) model was utilized to specify the Gibbs free energy of the proton-electron pair as the function of electrical potential.[5, 6] We applied in this work the same free energy corrections for the gaseous species and solvation effect as in Refs.[7, 8]

Considering that the CO_2RR was carried out at aqueous phase condition, a ceria cluster (Ce_3O_7) supported on Bi_2O_3 (100) surface is adopted to simulate the Bi_2O_3/CeO_x catalyst, denoted as $Ce_3O_7/Bi_2O_3(100)$.[9] Bi_2O_3 (100) surface was adopted to model the Bi_2O_3 catalyst for reference. Bi_2O_3 (100) substrate was modelled as a five-layered slab with (2×2) unit cells, of which the bottom three layers were fixed. The top two layers of Bi_2O_3 (100), the CeO_7 cluster and the surface species were fully relaxed. A vacuum spacing of 15 Å along the normal direction (z) to the surface and a 3×3×1 Gamma centered k-point sampling was used for the models.

Supplementary figures

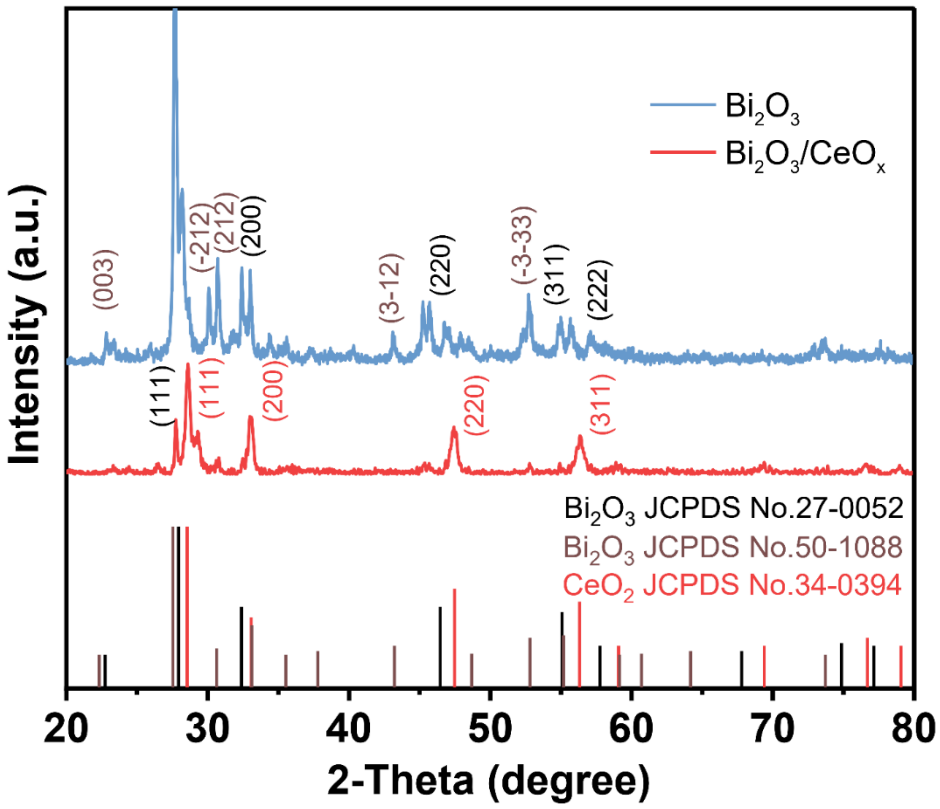

Figure S1. XRD pattern of Bi_2O_3/CeO_x.

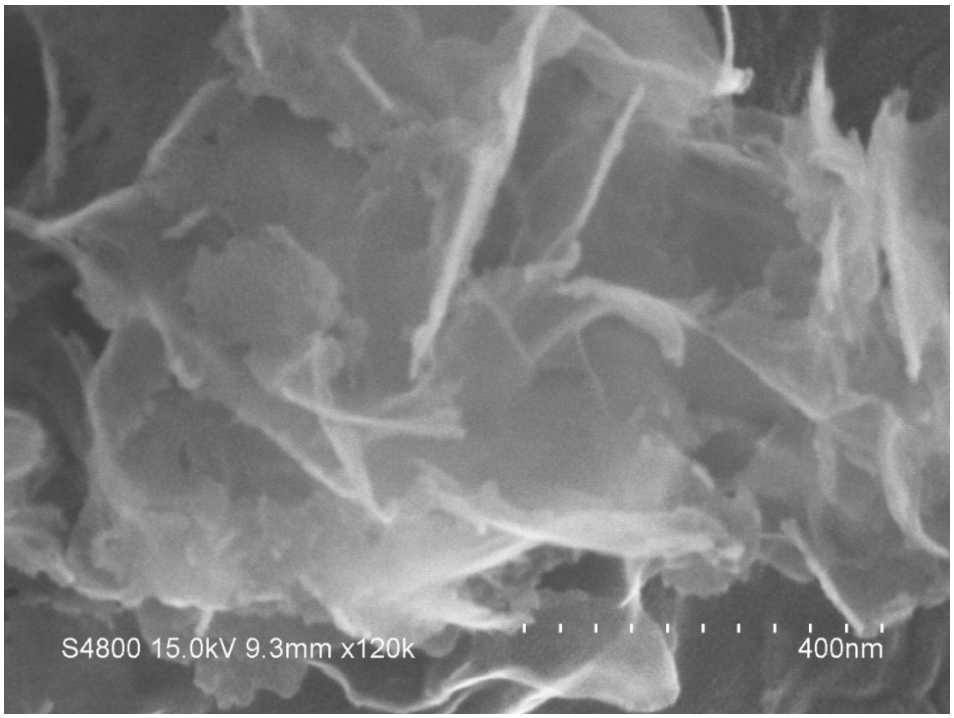

Figure S2. SEM image of Bi_2O_3.

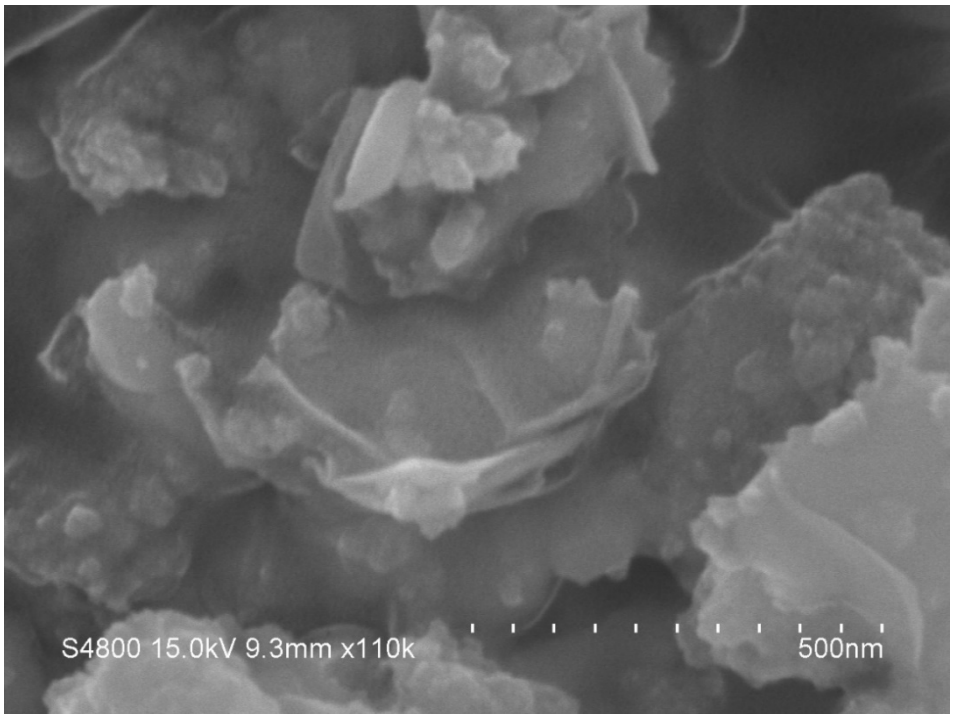

Figure S3. SEM image of Bi_2O_3/CeO_x.

SEM image shows that the ultrathin nanosheet structure of Bi_2O_3 does not change after the addition of CeO_x, and it can be clearly seen that CeO_x nanoparticles are successfully loaded on the Bi_2O_3 nanosheet.

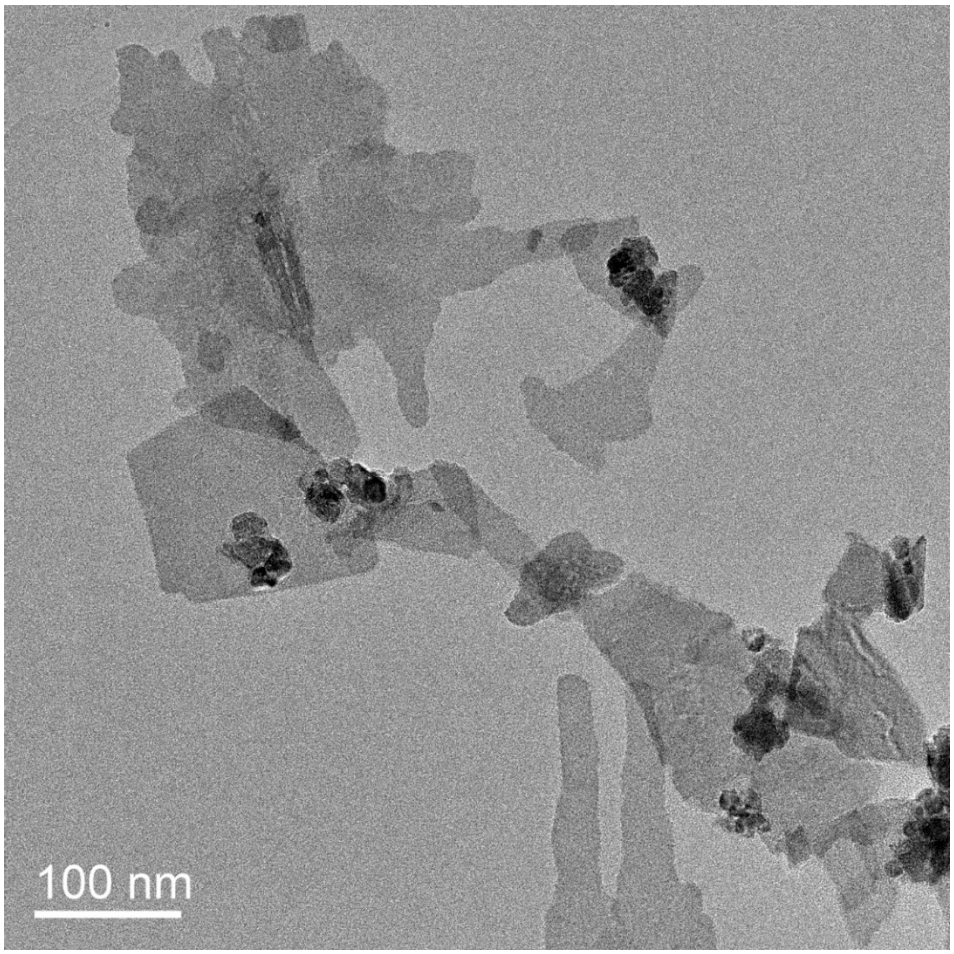

Figure S4. TEM image of Bi_2O_3/CeO_x.

TEM image shows that Bi_2O_3 exhibits an irregular nanosheet structure and CeO_x particles are loaded on the surface of the nanosheets, showing strong lining differences.

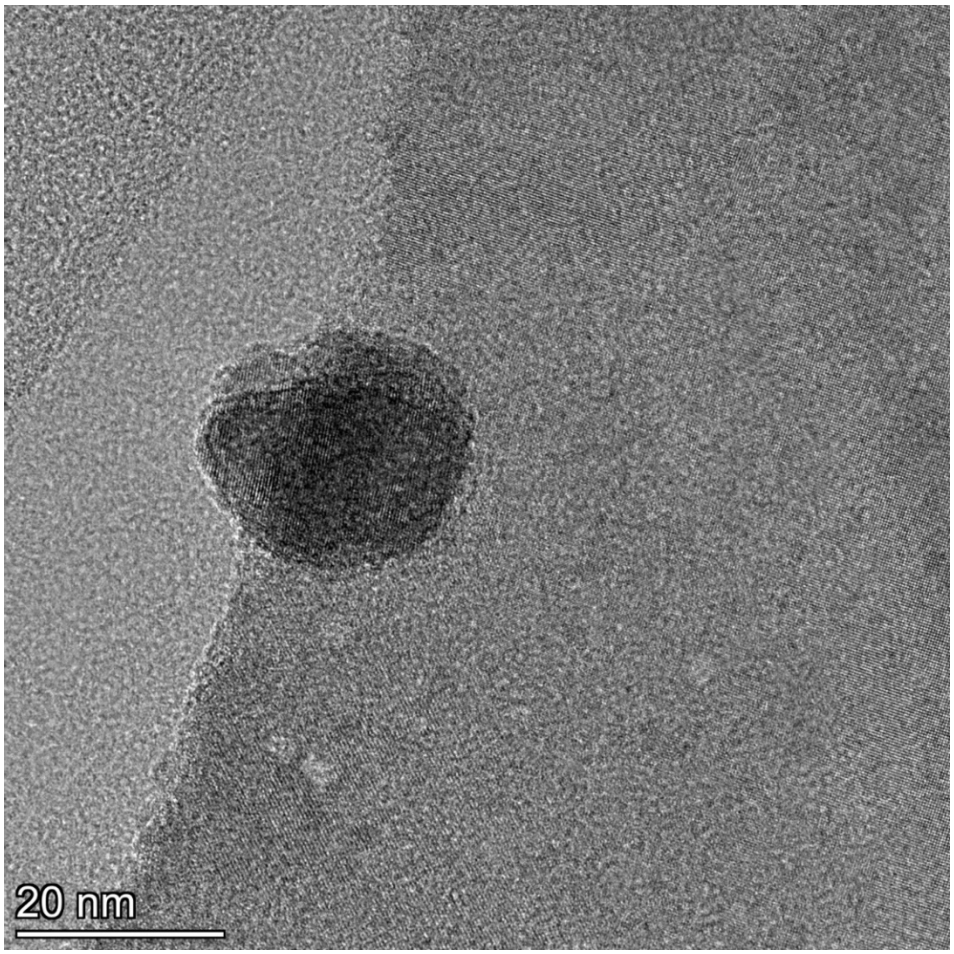

Figure S5. TEM image of Bi_2O_3/CeO_x.

TEM image shows that the particle size of CeO_x nanoparticles is around 20 nm.

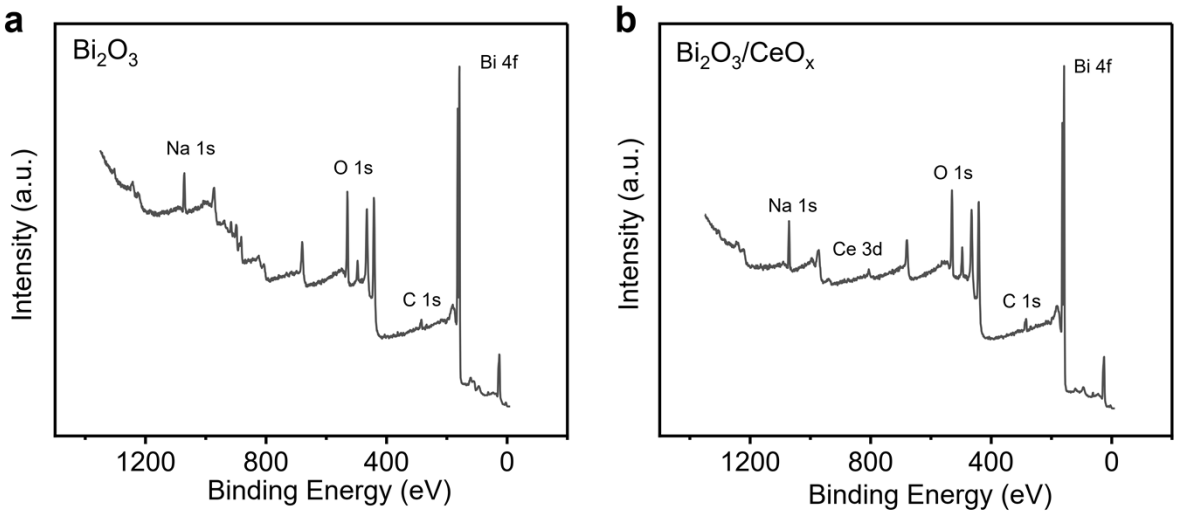

Figure S6. XPS spectra of Bi_2O_3 and Bi_2O_3/CeO_x.

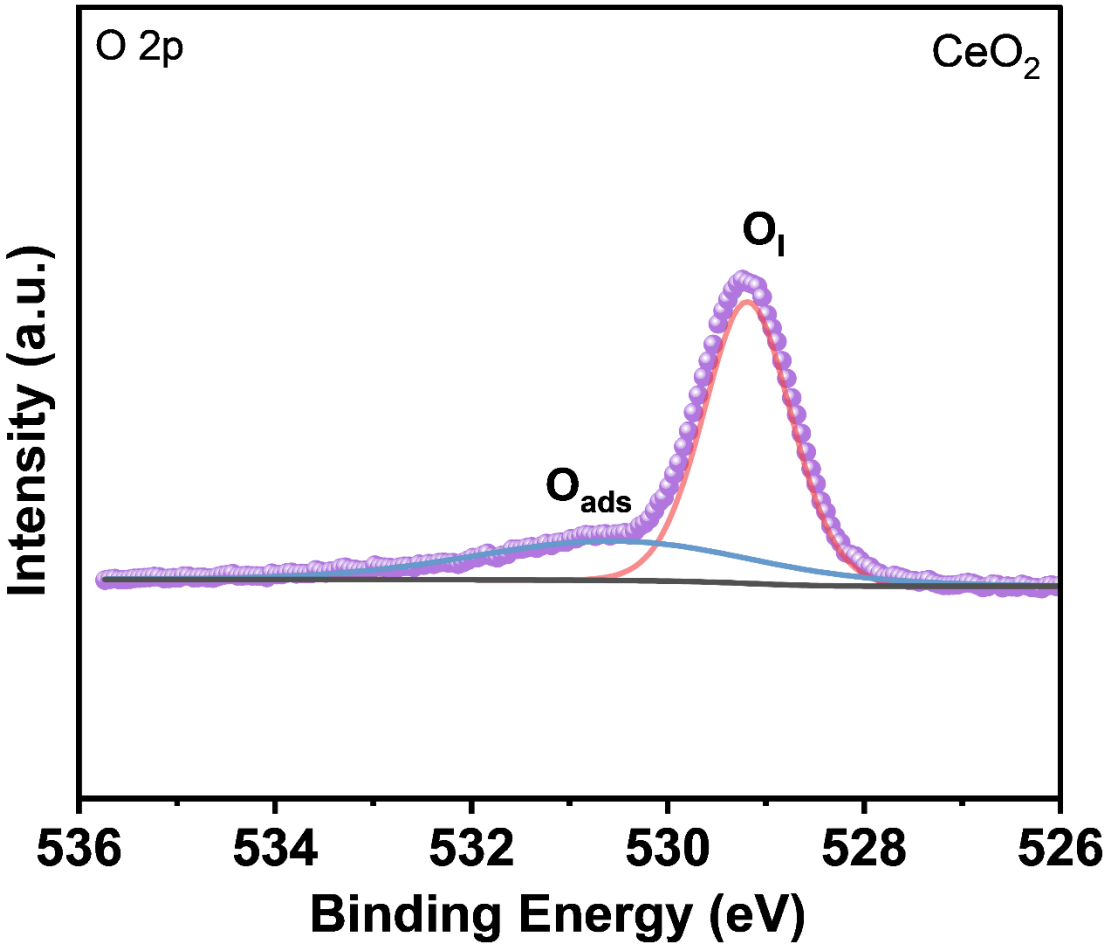

Figure S7. XPS O1s spectra of CeO_x.

The O1s spectrum of CeO_x showed that the peak O_{ads} around 531.3 eV belongs to the peak of oxygen vacancy, which proved that the oxygen vacancy of Bi_2O/CeO_x heterostructures came from CeO_x rather than Bi_2O_3.

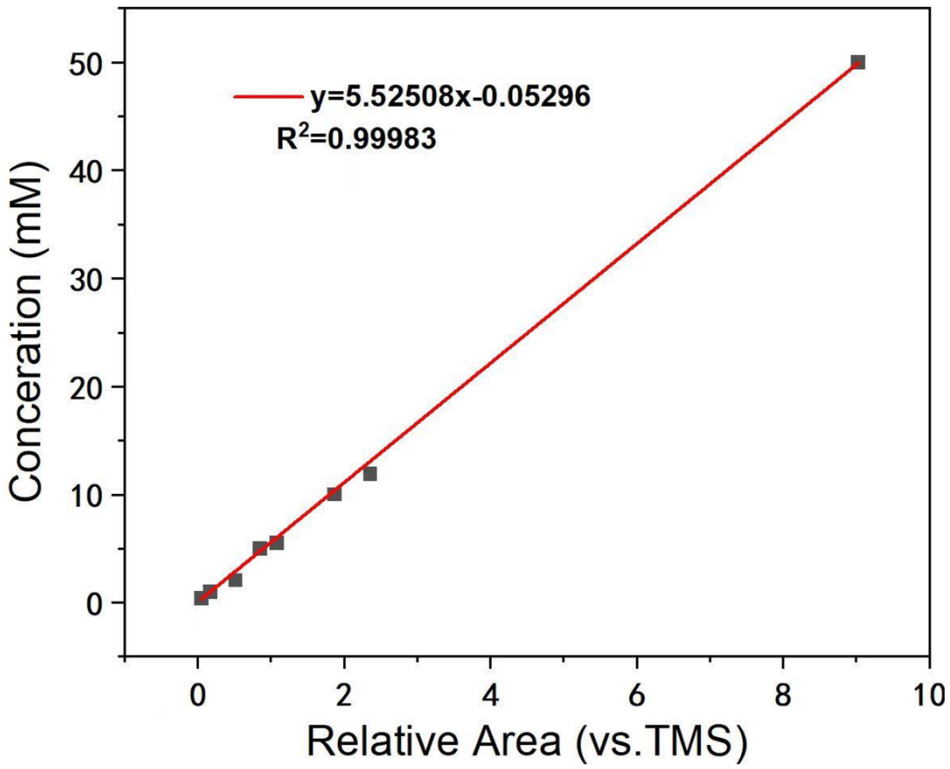

Figure S8. Calibration curve for standard HCOOK solutions by using 0.05% tetramethylsilane (TMS) as internal standard.

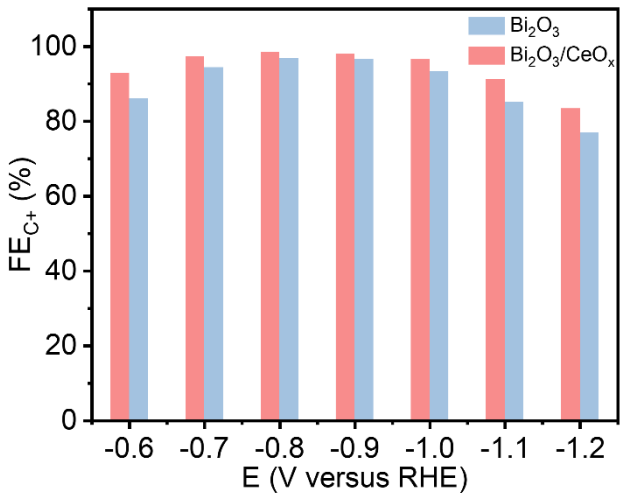

Figure S9. FE of carbon-containing product at multiple voltages.

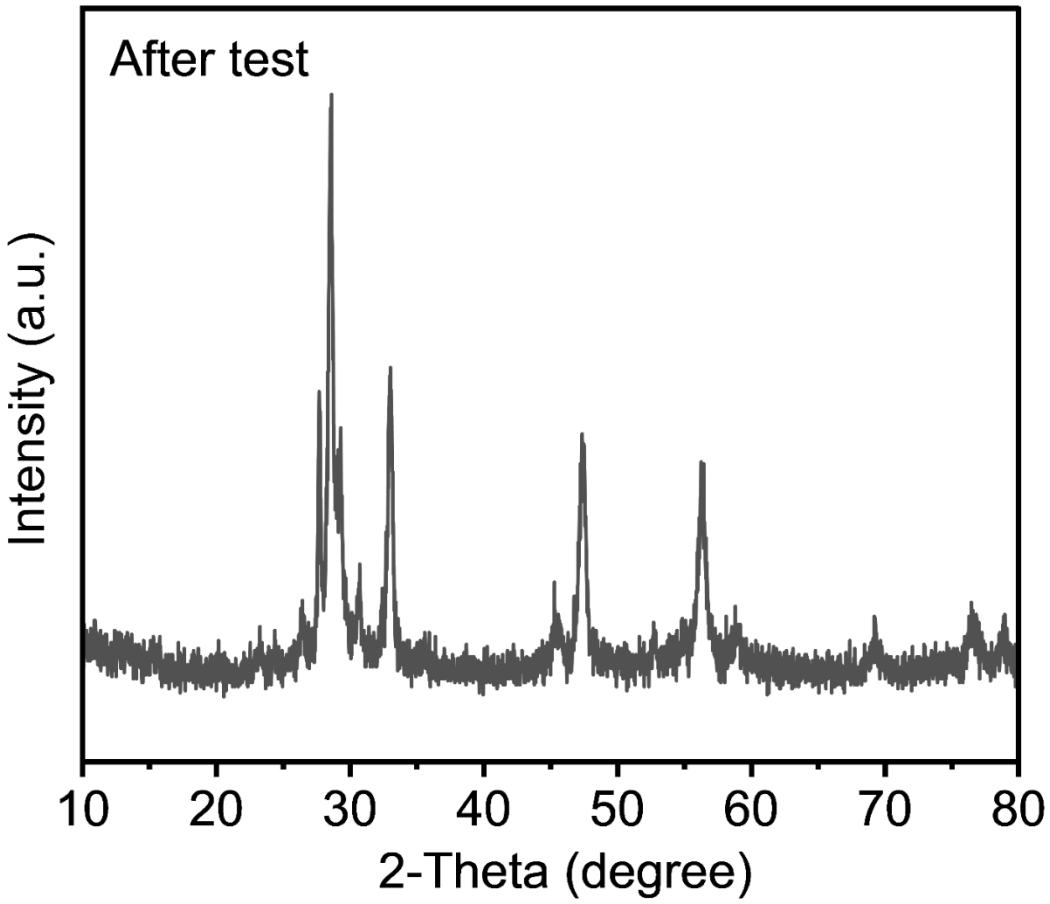

Figure S10. X-ray diffraction pattern of Bi_2O_3/CeO_x catalyst after stability testing.

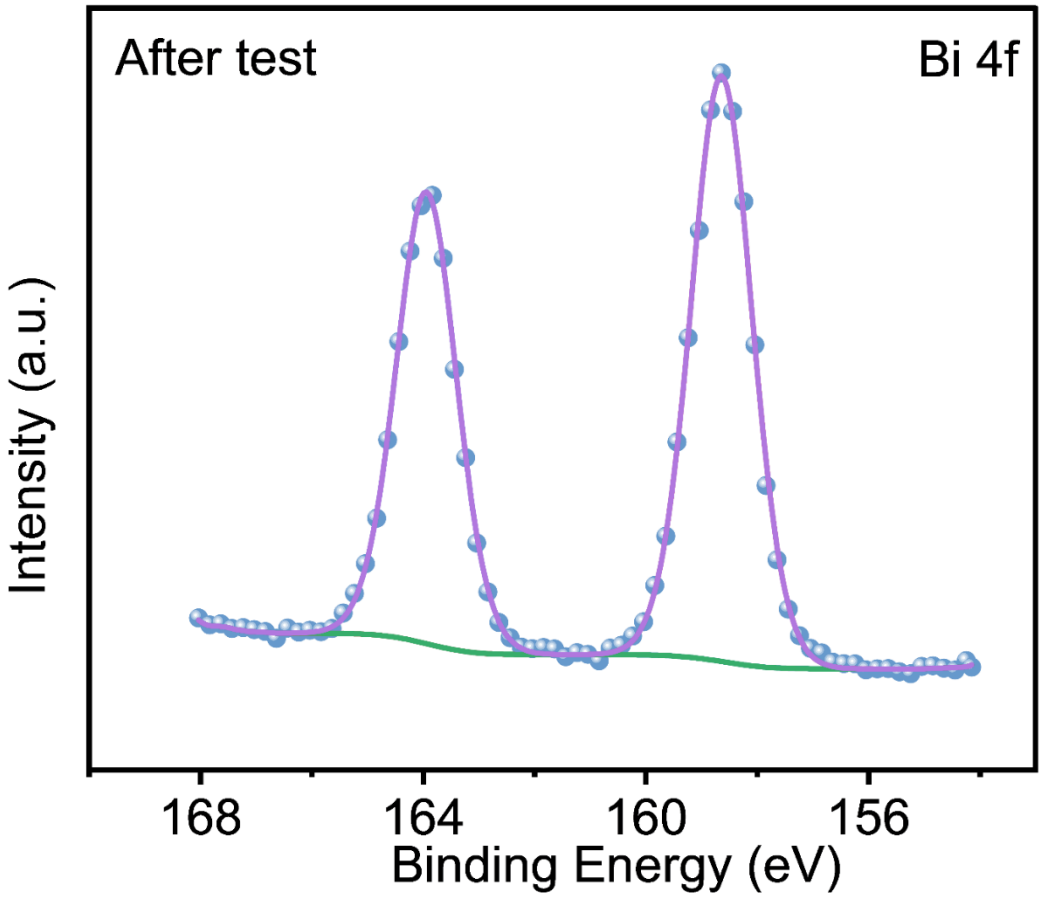

Figure S11. XPS Bi 4f spectrum of Bi_2O_3/CeO_x catalyst after stability testing.

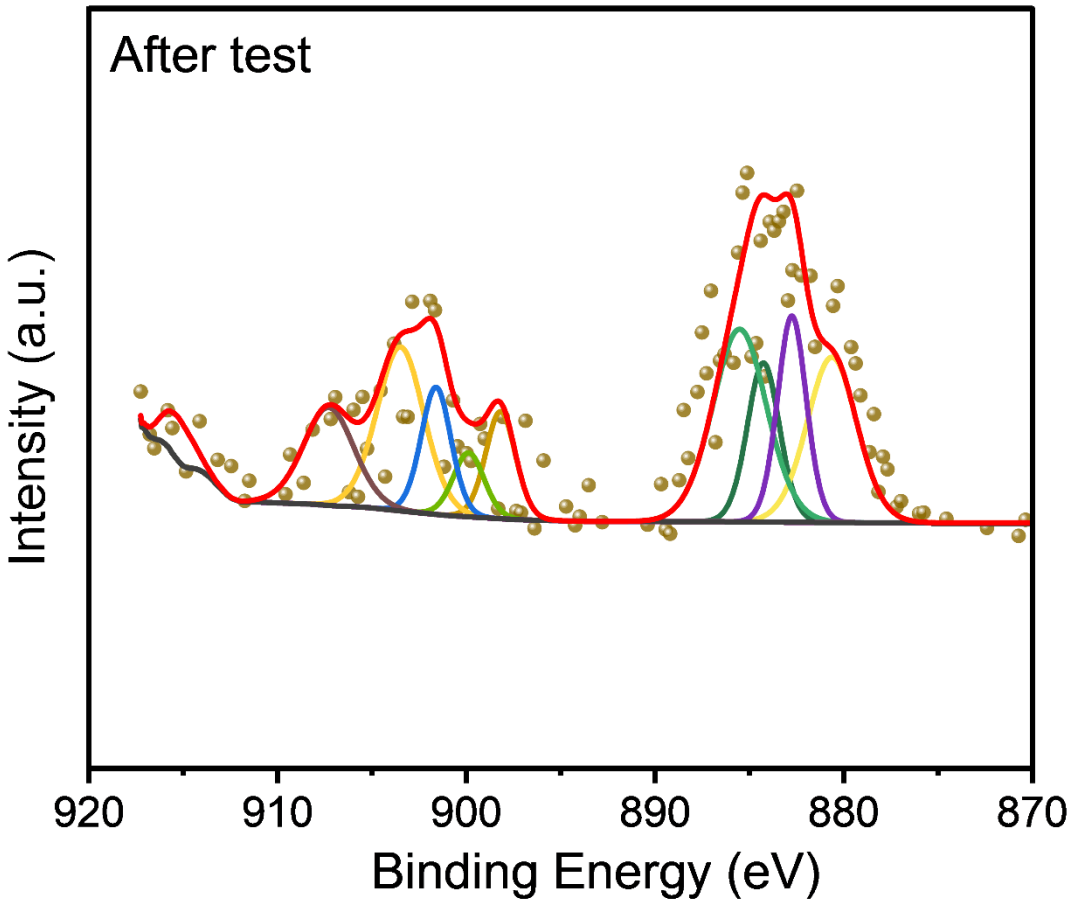

Figure S12. XPS Ce 3d spectrum of Bi_2O_3/CeO_x catalyst after stability testing.

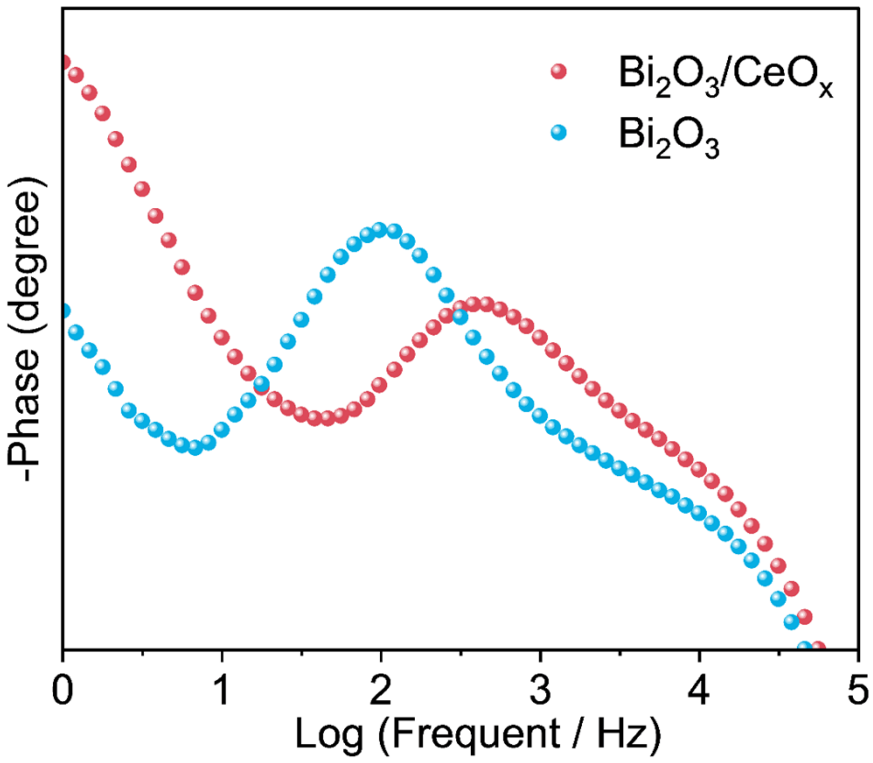

Figure S13. Bode plots of Bi_2O_3 and Bi_2O_3/CeO_x.

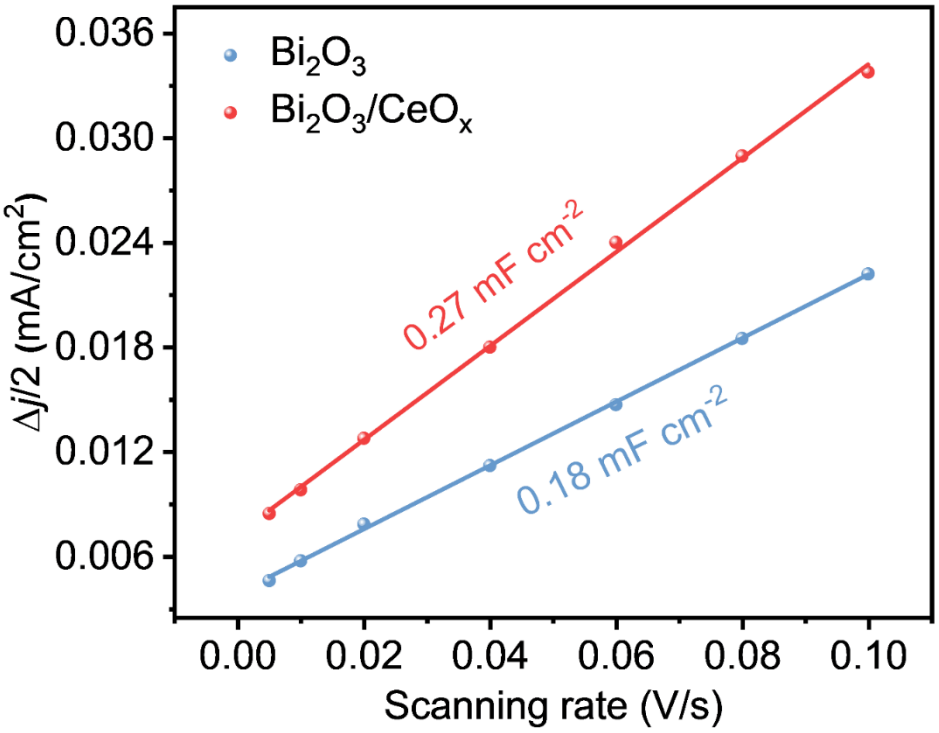

Figure S14. Electrochemical active surface area (ESCA) curve for Bi_2O_3 and Bi_2O_3/CeO_x.

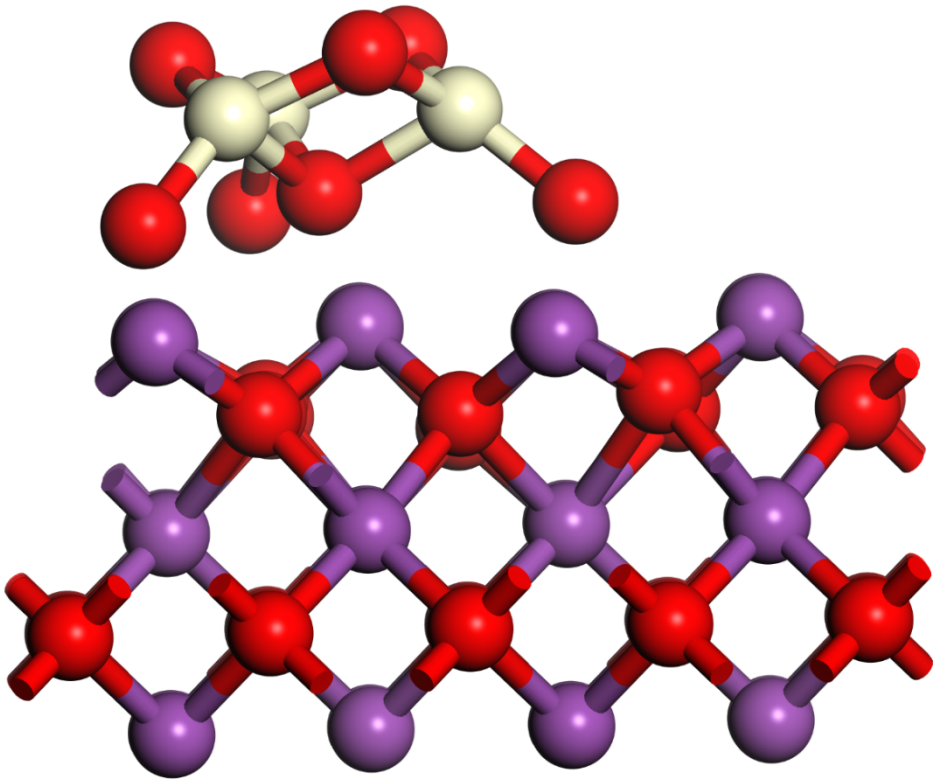

Figure S15. Stable model of density function theory (DFT) calculation for Bi_2O_3/CeO_x.

Supplementary tables

Table S1† Comparison of the performance of various Bi-based catalysts for CO_2 electroreduction to formate.

Catalyst	$FE_{formate}$ (%)	$j_{formate}$ (mA cm^{-2})	Reference
Bi_2O_3@C-800	92	6.9	Angew. Chem. Int. Ed. 2020, 59, 10807–10813.
Bi_2O_3-NGQDs	98.1	18.1	Angew. Chem. Int. Ed. 2018, 57, 12790–12794.
Bi–Cu_2S	92.4	~17.5	Nanoscale Horizons 2022,7,518-514.
Bi@Bi_2O_3	~100	22.4	Science Bulletin. 2020, 65, 1635-1642.
Bi_2S_3-Bi_2O_3 NSs	93.8	17.1	Small 2022, 18, 2105682
Bi_2O_3NSs@MCCM	93.8	17.7	Angew. Chem. Int. Ed. 2019, 58, 13828.
Bi-300	104.33	8.04	Angew. Chem. Int. Ed. 2020, 59, 20112–20119
Bi_2Te_3 NPs/C	89.6	13	Adv. Mater. 2020, 32, 1906477
Bi-ene	97.45	14.6	Angew. Chem. Int. Ed. 2020, 59, 15014–15020
f-Bi_2O_3	87	20.9	Adv. Funct. Mater. 2020, 30, 1906478
Bi_2O_3/CeO_x	98.28	45	This work

References

1 B. Delley, *The Journal of Chemical Physics*, 2000, **113**, 7756-7764.
2 J. P. Perdew, K. Burke and M. Ernzerhof, *Physical Review Letters*, 1996, **77**, 3865-3868.
3 A. Klamt, V. Jonas, T. Bürger and J. C. W. Lohrenz, *The Journal of Physical Chemistry A*, 1998, **102**, 5074-5085.
4 B. Delley, *Physical Review B*, 2002, **66**, 155125.
5 J. K. Nørskov, J. Rossmeisl, A. Logadottir, L. Lindqvist, J. R. Kitchin, T. Bligaard and H. Jónsson, *The Journal of Physical Chemistry B*, 2004, **108**, 17886-17892.
6 A. A. Peterson, F. Abild-Pedersen, F. Studt, J. Rossmeisl and J. K. Nørskov, *Energy & Environmental Science*, 2010, **3**, 1311-1315.
7 W. Luo, W. Xie, R. Mutschler, E. Oveisi, G. L. De Gregorio, R. Buonsanti and A. Züttel, *ACS Catalysis*, 2018, **8**, 6571-6581.
8 W. Ma, S. Xie, X.-G. Zhang, F. Sun, J. Kang, Z. Jiang, Q. Zhang, D.-Y. Wu and Y. Wang, *Nature Communications*, 2019, **10**, 892.
9 D. Gao, Y. Zhang, Z. Zhou, F. Cai, X. Zhao, W. Huang, Y. Li, J. Zhu, P. Liu, F. Yang, G. Wang and X. Bao, *Journal of the American Chemical Society*, 2017, **139**, 5652-5655.